

Two- and three-pion finite-volume spectra at maximal isospin from lattice QCD

Ben Hörz*

Nuclear Science Division, Lawrence Berkeley National Laboratory, Berkeley, CA 94720, USA

Andrew Hanlon†

Helmholtz-Institut Mainz, Johannes Gutenberg-Universität, 55099 Mainz, Germany

(Dated: October 8, 2019)

We present the three-pion spectrum with maximal isospin in a finite volume determined from lattice QCD, including excited states in addition to the ground states across various irreducible representations at zero and nonzero total momentum. The required correlation functions, from which the spectrum is extracted, are computed using a newly implemented algorithm which speeds up the computation by more than an order of magnitude. On a subset of the data we extract a nonzero value of the three-pion threshold scattering amplitude using the $1/L$ expansion of the three-particle quantization condition, which consistently describes all states at zero total momentum. The finite-volume spectrum is publicly available to facilitate further explorations within the available three-particle finite-volume approaches.

INTRODUCTION

Lattice QCD calculations of scattering amplitudes have matured significantly over the last decade owing to marked increases in available computational capacity and improved algorithms. A widely used approach for constraining scattering observables from simulations relies on precise measurements of the interacting energy levels of QCD in a finite volume, which encode hadron interactions via the shifts from their noninteracting values [1–5] (see [6] for a survey of extensions of the formalism and numerical results).

So far, practical calculations in lattice QCD have been mostly confined to the two-hadron sector. Though a large abundance of lattice data is currently available for scattering of two hadrons (e.g. $\pi\pi$ scattering in all three isospin channels [7–31], see also [32, 33] for results using a potential-based approach), these calculations are formally restricted to energies below thresholds involving three or more hadrons due to the use of a formalism for relating finite-volume spectra to scattering amplitudes that is limited to two-hadron scattering. This limitation has precluded a proper lattice QCD study of systems involving three or more stable hadrons at light pion masses, e.g. the Roper resonance which decays to both two- and three-particle channels, the $\omega(782)$ decaying to three pions, many of the X , Y and Z resonances, and three-nucleon interactions relevant for nuclear physics.

Following the demonstration that the finite-volume spectrum is determined by the infinite-volume S matrix, even in the presence of three-particle intermediate states [34], significant progress has been made in developing the necessary formalism to interpret the three-particle finite-volume spectrum, both by extending the two-particle derivation to include three-hadron states [35–38], as well as through alternative approaches [39–43] (for a review see [44]).[45] Thus, although the three-particle formalism is quite mature—including numerical explorations of the

corresponding quantization conditions [46–48]—data for three-particle finite-volume QCD spectra is lacking, since previous lattice QCD calculations have been restricted to the extraction of multi-meson ground states at rest [49–51]. Recently a first calculation of finite-volume spectra including three-particle energies was carried out in the b_1 system, whose results are however not yet amenable to an interpretation in the present three-particle formalisms [52]. Hence no comprehensive data exists to apply the available finite-volume formalisms.

We fill this gap by providing the two-pion and three-pion spectra with maximum isospin in various irreducible representations (irreps) at zero and nonzero total momentum in the elastic region, i.e. for center-of-mass energies E_{cm}/m_π below 4 and 5 for isospin $I = 2$ and $I = 3$ respectively. Our analysis of a subset of the data indicates sensitivity to the three-pion interaction at the current level of precision. In order to facilitate a more detailed exploration, possibly including the effect of higher partial waves [35, 36, 43, 53], the spectrum data is made public including all correlations.

A technical challenge concerns the growing number of Wick contractions required to compute correlation functions of suitable interpolating operators—from which the spectrum is extracted—as the number of valence quark fields increases. The continued need for improved algorithms to perform these contractions was pointed out recently [54] and indeed was a limiting factor in a recent study of meson-baryon scattering in the Δ channel [55]. While Refs. [56–61] investigated efficient contraction algorithms at the quark level, we employ the stochastic variant [62] of distillation [63] to treat quark propagation. In this framework, it is useful to view the correlation function construction in terms of contractions of tensors associated with the involved hadrons. Then, to reduce the operation count required to evaluate all contractions, we use a method which is well-known in quantum chemistry [64–66] and has attracted renewed interest in the

context of tensor networks [67]. The proposed optimization achieves a speedup by more than an order of magnitude, can be readily used for general physical systems (e.g. three-meson systems at nonmaximal isospin and two-baryon systems), and its implementation is publicly available [68].

This letter is organized as follows: We first discuss the interpolating operators employed and construction of their correlation functions, followed by a description of the ensemble used in this work. Subsequently the finite-volume spectra and extraction of two- and three-pion scattering parameters from a subset of the data are presented.

LATTICE QCD METHODS

Interpolating operators: Lattice simulations of QCD in a cubic box break the infinite-volume $SO(3)$ rotational symmetry. The spectrum in finite volume is customarily extracted employing interpolating operators which transform irreducibly under the symmetries of a cubic spatial lattice, i.e. the octahedral group O_h for zero total momentum $\mathbf{P} = \mathbf{0}$ and the corresponding little groups for $\mathbf{P} \neq \mathbf{0}$ [15, 69]. Correlation functions of such interpolators access only the sub-block of the finite-volume Hamiltonian corresponding to the same irrep, thus greatly simplifying the determination of the spectrum and the subsequent scattering-amplitude analysis.

We employ the simplest single-pion operator destroying a three-momentum \mathbf{p} given by

$$\pi_{\mathbf{p}}(t) = \sum_{\mathbf{x}} e^{-i\mathbf{p}\cdot\mathbf{x}} \bar{d}(\mathbf{x}, t) \gamma_5 u(\mathbf{x}, t). \quad (1)$$

This operator transforms in the A_{1u}^- and A_2^- irrep for zero and nonzero momentum respectively, where the superscript specifies the G -parity.

Two-pion interpolators which transform according to the irrep Λ of the little group of total momentum \mathbf{P} are obtained by forming appropriate linear combinations of two single-pion interpolators with momenta $\mathbf{p}_1 + \mathbf{p}_2 = \mathbf{P}$,

$$\pi\pi^{(\mathbf{P}, \Lambda)}(t) = c_{\mathbf{p}_1, \mathbf{p}_2}^{(\mathbf{P}, \Lambda)} \pi_{\mathbf{p}_1}(t) \pi_{\mathbf{p}_2}(t). \quad (2)$$

The relevant Clebsch-Gordan coefficients $c_{\mathbf{p}_1, \mathbf{p}_2}^{(\mathbf{P}, \Lambda)}$ were worked out in [69] (see also [15]) and used previously to study $\pi\pi$ scattering [22, 29].

Three-pion interpolators are obtained by iterating this process, i.e. by first coupling two of the pions into an intermediate irrep, then using the Clebsch-Gordan coefficients again to obtain operators transforming according to one of the total irreps of interest,

$$\pi\pi\pi^{(\mathbf{P}, \Lambda)}(t) = c_{\mathbf{p}_1, \mathbf{p}_2, \mathbf{p}_3}^{(\mathbf{P}, \Lambda)} \pi_{\mathbf{p}_1}(t) \pi_{\mathbf{p}_2}(t) \pi_{\mathbf{p}_3}(t). \quad (3)$$

Due to the weak interaction in $I = 2$ $\pi\pi$ scattering, which is the only relevant subprocess for this work, the more

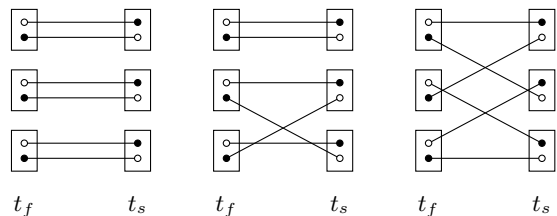


FIG. 1. Different topologies of Wick contractions required to evaluate $I = 3$ three-pion correlation functions. Circles indicate quark and antiquark fields tied into meson functions shown as boxes, which are subsequently contracted. Two-pion $I = 2$ Wick contractions appear as subexpressions.

elaborate operator construction discussed in [52] is not required. The interpolators we use in this work are listed in the supplemental material.

Correlation function construction: Quark propagation is treated using the stochastic LapH method [62] by first obtaining smeared solutions of the Dirac equation,

$$\varphi^{[r,d]} = \mathcal{S} D^{-1} \varrho^{[r,d]}, \quad (4)$$

for stochastic quark-field sources $\varrho^{[r,d]}$ with noise index $r = 1, \dots, N_\eta$, dilution [70, 71] index $d = 1, \dots, N_{\text{dil}}$, and where \mathcal{S} is the LapH smearing kernel, formed from the N_{ev} lowest eigenvectors of the three-dimensional covariant Laplacian. Next, useful intermediate quantities are the pion source and sink functions [62]

$$\begin{aligned} \mathcal{M}_{\mathbf{p}}^{[r_1, r_2, d_1, d_2]}(t) &= - \sum_{\mathbf{x}} e^{-i\mathbf{p}\cdot\mathbf{x}} \varrho_{a\alpha\mathbf{x}t}^{[r_1, d_1]*} \varrho_{a\alpha\mathbf{x}t}^{[r_2, d_2]}, \\ \bar{\mathcal{M}}_{\mathbf{p}}^{[r_1, r_2, d_1, d_2]}(t) &= \sum_{\mathbf{x}} e^{-i\mathbf{p}\cdot\mathbf{x}} \varphi_{a\alpha\mathbf{x}t}^{[r_1, d_1]*} \varphi_{a\alpha\mathbf{x}t}^{[r_2, d_2]}, \end{aligned} \quad (5)$$

with summed color index a and spin index α , and two open noise and dilution indices. In terms of these meson functions, the single-pion correlation function on a single gauge configuration is obtained by the average over noise combinations $\{r_1, r_2\}$ [62]

$$C_{\pi_{\mathbf{p}}}(t_f - t_s) \propto - \sum_{\{r_1, r_2\}} \bar{\mathcal{M}}_{\mathbf{p}}^{[r_1, r_2, d_1, d_2]}(t_f) \mathcal{M}_{\mathbf{p}}^{[r_1, r_2, d_1, d_2]*}(t_s), \quad (6)$$

with proper normalization given by the number of noise combinations used to perform the average.

For a given momentum, pair of source and sink time t_s and t_f , and noise combination, Eq. (6) is a tensor contraction over dilution indices of two rank-2 tensors with index range N_{dil} . Two- and three-pion correlation functions with maximal isospin can be computed using the same building blocks [62] and involve tensor contractions governed by all possible Wick contractions of four and six rank-2 tensors respectively.

The number of Wick contractions grows factorially as more pions are included [49], and the different topologies

TABLE I. Ensemble and measurement setup used in this work. Measurements are performed on N_{cfg} configurations with spatial volume L^3 separated by 4MDU. Correlation functions are estimated starting from a single source time $t_s/a = 35$ using N_η diluted noise sources to estimate quark propagators (see [62] for unexplained notation). Other parameters, e.g. for stout smearing [72], are the same as in [29].

am_π	L/a	N_{ev}	dilution	N_η	N_{cfg}
0.06504(33)	64	448	(TF,SF,LI16)	6	1100

of diagrams for three-pion correlation functions in the sector of maximal isospin are shown in Fig. 1. However, across the relevant diagrams there is a lot of redundancy which can be exploited systematically to reduce the number of arithmetic operations required for their evaluation. In particular, all diagrams required for the computation of $I = 2$ two-pion correlation functions appear as subdiagrams of $I = 3$ three-pion correlation functions.

The algorithm to automatically perform the operation-count minimization is described in the supplemental material together with a detailed example. For the evaluation of the correlation functions required in this work we achieve a speed-up by roughly a factor of 15.

Ensemble details: The results in this work are based on the D200 ensemble generated through the CLS effort [73] with $N_f = 2 + 1$ quark flavors at a pion mass $m_\pi \approx 200$ MeV and lattice spacing $a \approx 0.064$ fm [74]. The ensemble and measurement setup is detailed in Table I. In order to ensure a Hermitian matrix of correlation functions despite the use of open boundary conditions in the temporal direction [75], our interpolating operators are always separated from the temporal boundaries by at least t_s , where $m_\pi t_s = 2.2$.

Pion-pion scattering in the isovector channel has been investigated on this ensemble previously [29], and statistics subsequently improved considerably to provide spectroscopic information for the determination of the hadronic vacuum polarization on the same ensemble [76]. The pion functions are re-used from that work, and hence no additional meson functions or solutions of the Dirac equation have to be computed.

RESULTS

Analysis strategy: The procedure to extract the finite-volume spectrum from a matrix of correlation functions $C_{ij}(t)$ in a given irrep is discussed in detail in [22] and we use the analysis suite [77] developed in [29].

We solve a generalized eigenvalue problem [4, 78, 79] for a fixed reference time and diagonalization time ($t_0 = 5a, t_* = 10a$), corresponding to roughly 0.32 fm and 0.64 fm in physical units [74], in order to extract not only the ground state but also excited states in most irreps.

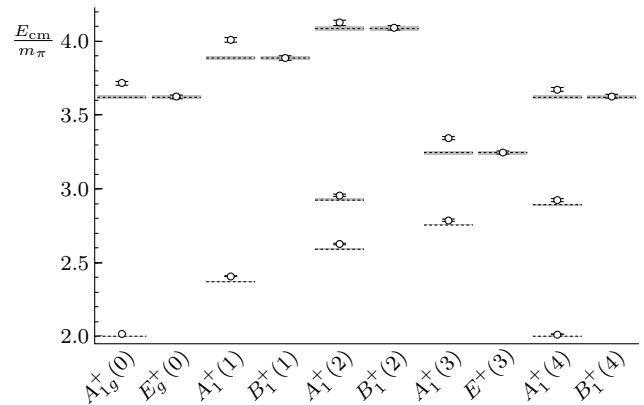


FIG. 2. $I = 2$ two-pion spectrum in various irreps $\Lambda(\mathbf{d}^2)$ with total momentum $\mathbf{P} = \frac{2\pi}{L}\mathbf{d}$. Open symbols denote the measured interacting energies which are shifted from their noninteracting values shown as dashed lines.

Results from different (t_0, t_*) are indistinguishable, presumably due to the weak interaction in $I = 2$ and $I = 3$ pion scattering which results in little mixing of our interpolating operators, in which each hadron has been projected to definite momentum and is hence expected to overlap predominantly with a single state.

For two-pion states the difference ΔE between interacting and noninteracting energies is determined from single-exponential fits at sufficiently large time separations to the ratios

$$R_i(t) = \frac{\hat{C}_{ii}(t)}{C_{\pi_{\mathbf{p}_1}}(t) C_{\pi_{\mathbf{p}_2}}(t)} \xrightarrow{\text{large } t} A e^{-\Delta E_i t} \quad (7)$$

of diagonal elements of the ‘optimized’ correlation matrix \hat{C} [22] and two single-pion correlation functions, and similarly for the three-pion states [49]. Absolute energies are reconstructed from those energy differences using the single-pion dispersion relation. The attainable precision is generally at the few-permille level for the energies measured in units of the single-pion mass.

Two-pion spectrum and scattering amplitude: The two-pion spectrum with maximal isospin is shown in Fig. 2 together with the noninteracting energies. The respective differences encode the two-pion scattering amplitude for $\ell = 0$ shown in Fig. 3 neglecting the effect of higher even partial waves. Its energy dependence for scattering momentum $q^2/m_\pi^2 < 1$ is described using the effective-range expansion

$$q \cot \delta_0 = -\frac{1}{a_0} + \frac{r_0}{2} q^2, \quad (8)$$

and the scattering length a_0 and effective range r_0 are determined from a fit using the determinant-residual method [80] with $\mu = 64$, which yields

$$m_\pi a_0 = 0.1019(88), \quad m_\pi r_0 = 9.0(2.4), \quad \chi^2/\text{dof} = 1.33. \quad (9)$$

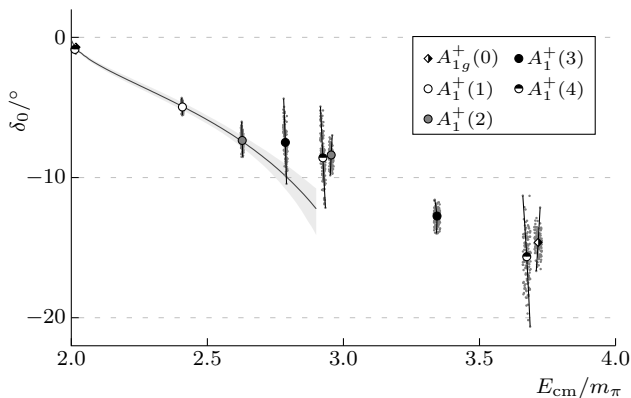


FIG. 3. Energy dependence of the $I = 2$ $\pi\pi$ s-wave scattering amplitude extracted from the two-pion spectrum. The gray band shows the result of the fit to the five leftmost points using the effective range expansion given in Eq. (8).

A comparison of our scattering length with previous lattice QCD determinations [7–9, 15, 17, 18, 22], together with the experimental value from [81], is shown in the supplemental material.

Three-pion spectrum and $1/L$ expansion: The three-pion spectrum with maximal isospin is shown in Fig. 4, displaying significant energy shifts in all irreps. In particular, interacting energy levels from different irreps that contain some degeneracy of the noninteracting spectra (e.g. A_{1u}^- and E_u^- at zero total momentum) differ substantially, which may suggest sensitivity to different combinations of low-energy scattering parameters.

At leading order in the $1/L$ expansion of the three-particle quantization condition [82–86] [87],

$$\begin{aligned} \Delta E_3 = & \frac{12\pi a_0}{m_\pi L^3} \left\{ 1 - \left(\frac{a_0}{\pi L}\right) \mathcal{I} + \left(\frac{a_0}{\pi L}\right)^2 (\mathcal{I}^2 + \mathcal{J}) + \frac{3\pi a_0}{m_\pi^2 L^3} \right. \\ & + \frac{64\pi^2 a_0^2 \mathcal{C}_3}{m_\pi L^3} + \frac{6\pi r_0 a_0^2}{L^3} + \left.\left(\frac{a_0}{\pi L}\right)^3 [c_L \log(N_{\text{cut}}) - \mathcal{I}^3 + \mathcal{I}\mathcal{J} \right. \\ & \left. \left. + 15\mathcal{K} + \mathcal{C}_F + \mathcal{C}_4 + \mathcal{C}_5\right] \right\} - \frac{\mathcal{M}_{3,\text{th}}}{48m_\pi^3 L^6} + O(L^{-7}), \quad (10) \end{aligned}$$

the ground-state energy shift ΔE_3 is three times larger than the corresponding two-particle shift ΔE_2 [49]. The deviation of our numerical result

$$\Delta E_3/\Delta E_2 = 2.78(21), \quad (11)$$

is due to two-particle effects at higher orders in $1/L$ and the three-pion interaction. Using the two-particle scattering length and effective range determined before, the three-particle threshold scattering amplitude entering at L^{-6} can be isolated and we obtain

$$\frac{m_\pi^2 \mathcal{M}_{3,\text{th}}}{48(m_\pi L)^6} = 0.0113(43). \quad (12)$$

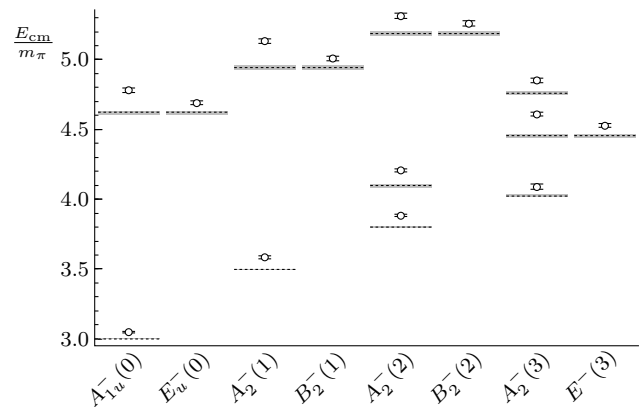


FIG. 4. Same as Fig. 2 but for the $I = 3$ three-pion spectrum.

While this quantity depends on how two- and three-particle effects are separated [47, 84], within the scheme discussed in those references our result indicates sensitivity to three-particle physics.

Using the nonrelativistic threshold expansion from Ref. [86] yields a result with similar significance. From that reference, the energy of the excited states at rest are predicted to be

$$\begin{aligned} A_{1u}^- : \quad E'_3/m_\pi &= 4.76(8), \\ E_u^- : \quad E'_3/m_\pi &= 4.72(2), \end{aligned} \quad (13)$$

in good agreement with our measured values. Further, the formalism employed in [48] with the scattering parameters determined there predicts the first excited state in the at-rest A_{1u}^- irrep to be [88]

$$E'_3/m_\pi = 4.75 \quad (14)$$

at our pion mass and spatial volume, which is also in agreement with the measured value.

More work along the lines of [43, 53] is required to apply the quantization condition to the energies in all irreps presented here. In order to facilitate further investigations in that direction, the two-pion and three-pion spectra are made publicly available including all correlations. The values and covariance matrix of all extracted energies, as well as the single-pion mass, are given in the supplemental material, and the bootstrap samples from this analysis are available as ancillary files with the arXiv submission.

CONCLUSIONS AND OUTLOOK

We have presented the $I = 3$ three-pion spectrum in finite volume from lattice QCD in which, for the first time, the excited states in various irreps at zero and nonzero total momentum have been extracted. The nonrelativistic three-particle $1/L$ expansion consistently describes the

levels in the irreps at zero total momentum. However, the entire spectrum should be interpreted in the framework of a full three-particle finite-volume formalism in order to corroborate and extend our extraction of the three-pion interaction. In the interest of facilitating those investigations, which will require generalizations of the formulae currently available in the literature, all spectra are made public, including their correlations.

We also described a method to reduce the computational cost of constructing correlation functions in the stochastic variant of distillation, achieving a speedup of more than an order of magnitude for the set of observables considered here. This algorithmic improvement paves the way to study more complicated systems such as the Roper resonance, which has a sizable branching ratio for decays to $N\pi\pi$ as well as $N\pi$, and also reduces the computational cost associated with correlation function construction for baryon-baryon systems, which will facilitate the lattice QCD investigation of nucleon-nucleon as well as nucleon-hyperon interactions relevant for nuclear physics.

We acknowledge helpful discussions with Andria Agadjanov, John Bulava, Ken McElvain, Daniel Mohler, Colin Morningstar, Fernando Romero-López, Akaki Rusetzky, and André Walker-Loud. We thank Christopher Körber for useful comments on an earlier version of the manuscript. The authors thank the Yukawa Institute for Theoretical Physics at Kyoto University, where part of this work was performed during the YITP-19-01 workshop on “Frontiers in Lattice QCD and related topics”. The work of BH was supported by the Laboratory Directed Research and Development Program of Lawrence Berkeley National Laboratory under U.S. Department of Energy Contract No. DE-AC02-05CH11231. Calculations for this project were performed on the HPC clusters “HIMster II” at the Helmholtz-Institut Mainz and “Mogon II” at JGU Mainz. Our programs use the deflated SAP+GCR solver from the openQCD package [75], as well as the QDP++/Chroma libraries [89]. We are grateful to our colleagues in the CLS initiative for sharing ensembles.

* hoerz@lbl.gov

† ahanlon@uni-mainz.de

- [1] M. Luscher, Commun. Math. Phys. **104**, 177 (1986).
- [2] M. Luscher, Commun. Math. Phys. **105**, 153 (1986).
- [3] M. Lüscher, Nucl. Phys. **B354**, 531 (1991).
- [4] M. Luscher and U. Wolff, Nucl. Phys. **B339**, 222 (1990).
- [5] K. Rummukainen and S. A. Gottlieb, Nucl. Phys. **B450**, 397 (1995), arXiv:hep-lat/9503028 [hep-lat].
- [6] R. A. Briceño, J. J. Dudek, and R. D. Young, (2017), arXiv:1706.06223 [hep-lat].
- [7] S. R. Beane, P. F. Bedaque, K. Orginos, and M. J. Savage (NPLQCD), Phys. Rev. **D73**, 054503 (2006), arXiv:hep-lat/0506013 [hep-lat].
- [8] S. R. Beane, T. C. Luu, K. Orginos, A. Parreno, M. J. Savage, A. Torok, and A. Walker-Loud, Phys. Rev. **D77**, 014505 (2008), arXiv:0706.3026 [hep-lat].
- [9] X. Feng, K. Jansen, and D. B. Renner, Phys. Lett. **B684**, 268 (2010), arXiv:0909.3255 [hep-lat].
- [10] X. Feng, K. Jansen, and D. B. Renner, Phys. Rev. **D83**, 094505 (2011), arXiv:1011.5288 [hep-lat].
- [11] S. R. Beane, E. Chang, W. Detmold, H. W. Lin, T. C. Luu, K. Orginos, A. Parreno, M. J. Savage, A. Torok, and A. Walker-Loud (NPLQCD), Phys. Rev. **D85**, 034505 (2012), arXiv:1107.5023 [hep-lat].
- [12] C. B. Lang, D. Mohler, S. Prelovsek, and M. Vidmar, Phys. Rev. **D84**, 054503 (2011), [Erratum: Phys. Rev. **D89**, no.5, 059903(2014)], arXiv:1105.5636 [hep-lat].
- [13] S. Aoki *et al.* (CS), Phys. Rev. **D84**, 094505 (2011), arXiv:1106.5365 [hep-lat].
- [14] C. Pelissier and A. Alexandru, Phys. Rev. **D87**, 014503 (2013), arXiv:1211.0092 [hep-lat].
- [15] J. J. Dudek, R. G. Edwards, and C. E. Thomas, Phys. Rev. **D86**, 034031 (2012), arXiv:1203.6041 [hep-ph].
- [16] J. J. Dudek, R. G. Edwards, and C. E. Thomas (Hadron Spectrum), Phys. Rev. **D87**, 034505 (2013), arXiv:1212.0830 [hep-ph].
- [17] K. Sasaki, N. Ishizuka, M. Oka, and T. Yamazaki (PACS-CS), Phys. Rev. **D89**, 054502 (2014), arXiv:1311.7226 [hep-lat].
- [18] Z. Fu, Phys. Rev. **D87**, 074501 (2013), arXiv:1303.0517 [hep-lat].
- [19] D. J. Wilson, R. A. Briceño, J. J. Dudek, R. G. Edwards, and C. E. Thomas, Phys. Rev. **D92**, 094502 (2015), arXiv:1507.02599 [hep-ph].
- [20] C. Helmes, C. Jost, B. Knippschild, C. Liu, J. Liu, L. Liu, C. Urbach, M. Ueding, Z. Wang, and M. Werner (ETM), JHEP **09**, 109 (2015), arXiv:1506.00408 [hep-lat].
- [21] G. S. Bali, S. Collins, A. Cox, G. Donald, M. Göckeler, C. B. Lang, and A. Schäfer (RQCD), Phys. Rev. **D93**, 054509 (2016), arXiv:1512.08678 [hep-lat].
- [22] J. Bulava, B. Fahy, B. Hörz, K. J. Juge, C. Morningstar, and C. H. Wong, Nucl. Phys. **B910**, 842 (2016), arXiv:1604.05593 [hep-lat].
- [23] D. Guo, A. Alexandru, R. Molina, and M. Dring, Phys. Rev. **D94**, 034501 (2016), arXiv:1605.03993 [hep-lat].
- [24] Z. Fu and L. Wang, Phys. Rev. **D94**, 034505 (2016), arXiv:1608.07478 [hep-lat].
- [25] R. A. Briceño, J. J. Dudek, R. G. Edwards, and D. J. Wilson, Phys. Rev. Lett. **118**, 022002 (2017), arXiv:1607.05900 [hep-ph].
- [26] L. Liu *et al.*, Phys. Rev. **D96**, 054516 (2017), arXiv:1612.02061 [hep-lat].
- [27] C. Alexandrou, L. Leskovec, S. Meinel, J. Negele, S. Paul, M. Petschlies, A. Pochinsky, G. Rendon, and S. Syritsyn, Phys. Rev. **D96**, 034525 (2017), arXiv:1704.05439 [hep-lat].
- [28] R. A. Briceño, J. J. Dudek, R. G. Edwards, and D. J. Wilson, Phys. Rev. **D97**, 054513 (2018), arXiv:1708.06667 [hep-lat].
- [29] C. Andersen, J. Bulava, B. Hörz, and C. Morningstar, Nucl. Phys. **B939**, 145 (2019), arXiv:1808.05007 [hep-lat].
- [30] D. Guo, A. Alexandru, R. Molina, M. Mai, and M. Döring, Phys. Rev. **D98**, 014507 (2018), arXiv:1803.02897 [hep-lat].
- [31] C. Culver, M. Mai, A. Alexandru, M. Dring, and F. X. Lee, Phys. Rev. **D100**, 034509 (2019), arXiv:1905.10202

- [hep-lat].
- [32] T. Kurth, N. Ishii, T. Doi, S. Aoki, and T. Hatsuda, *JHEP* **12**, 015 (2013), arXiv:1305.4462 [hep-lat].
- [33] Y. Akahoshi, S. Aoki, T. Aoyama, T. Doi, T. Miyamoto, and K. Sasaki, (2019), arXiv:1904.09549 [hep-lat].
- [34] K. Polejaeva and A. Rusetsky, *Eur. Phys. J.* **A48**, 67 (2012), arXiv:1203.1241 [hep-lat].
- [35] M. T. Hansen and S. R. Sharpe, *Phys. Rev.* **D90**, 116003 (2014), arXiv:1408.5933 [hep-lat].
- [36] M. T. Hansen and S. R. Sharpe, *Phys. Rev.* **D92**, 114509 (2015), arXiv:1504.04248 [hep-lat].
- [37] R. A. Briceño, M. T. Hansen, and S. R. Sharpe, *Phys. Rev.* **D95**, 074510 (2017), arXiv:1701.07465 [hep-lat].
- [38] R. A. Briceño, M. T. Hansen, and S. R. Sharpe, *Phys. Rev.* **D99**, 014516 (2019), arXiv:1810.01429 [hep-lat].
- [39] D. Agadjanov, M. Doring, M. Mai, U.-G. Meißner, and A. Rusetsky, *JHEP* **06**, 043 (2016), arXiv:1603.07205 [hep-lat].
- [40] H.-W. Hammer, J.-Y. Pang, and A. Rusetsky, *JHEP* **09**, 109 (2017), arXiv:1706.07700 [hep-lat].
- [41] H. W. Hammer, J. Y. Pang, and A. Rusetsky, *JHEP* **10**, 115 (2017), arXiv:1707.02176 [hep-lat].
- [42] M. Mai and M. Döring, *Eur. Phys. J.* **A53**, 240 (2017), arXiv:1709.08222 [hep-lat].
- [43] M. Döring, H. W. Hammer, M. Mai, J. Y. Pang, A. Rusetsky, and J. Wu, *Phys. Rev.* **D97**, 114508 (2018), arXiv:1802.03362 [hep-lat].
- [44] M. T. Hansen and S. R. Sharpe, (2019), arXiv:1901.00483 [hep-lat].
- [45] See also [90–92] for a complementary approach for inclusive observables.
- [46] R. A. Briceño, M. T. Hansen, and S. R. Sharpe, *Phys. Rev.* **D98**, 014506 (2018), arXiv:1803.04169 [hep-lat].
- [47] F. Romero-López, A. Rusetsky, and C. Urbach, *Eur. Phys. J.* **C78**, 846 (2018), arXiv:1806.02367 [hep-lat].
- [48] M. Mai and M. Doring, *Phys. Rev. Lett.* **122**, 062503 (2019), arXiv:1807.04746 [hep-lat].
- [49] S. R. Beane, W. Detmold, T. C. Luu, K. Orginos, M. J. Savage, and A. Torok, *Phys. Rev. Lett.* **100**, 082004 (2008), arXiv:0710.1827 [hep-lat].
- [50] W. Detmold, M. J. Savage, A. Torok, S. R. Beane, T. C. Luu, K. Orginos, and A. Parreno, *Phys. Rev.* **D78**, 014507 (2008), arXiv:0803.2728 [hep-lat].
- [51] W. Detmold, K. Orginos, M. J. Savage, and A. Walker-Loud, *Phys. Rev.* **D78**, 054514 (2008), arXiv:0807.1856 [hep-lat].
- [52] A. J. Woss, C. E. Thomas, J. J. Dudek, R. G. Edwards, and D. J. Wilson, (2019), arXiv:1904.04136 [hep-lat].
- [53] T. D. Blanton, F. Romero-López, and S. R. Sharpe, *JHEP* **03**, 106 (2019), arXiv:1901.07095 [hep-lat].
- [54] W. Detmold, R. G. Edwards, J. J. Dudek, M. Engelhardt, H.-W. Lin, S. Meinel, K. Orginos, and P. Shanahan, (2019), arXiv:1904.09512 [hep-lat].
- [55] C. W. Andersen, J. Bulava, B. Hörz, and C. Morningstar, *Phys. Rev.* **D97**, 014506 (2018), arXiv:1710.01557 [hep-lat].
- [56] T. Yamazaki, Y. Kuramashi, and A. Ukawa (PACS-CS), *Phys. Rev.* **D81**, 111504 (2010), arXiv:0912.1383 [hep-lat].
- [57] W. Detmold and M. J. Savage, *Phys. Rev.* **D82**, 014511 (2010), arXiv:1001.2768 [hep-lat].
- [58] T. Doi and M. G. Endres, *Comput. Phys. Commun.* **184**, 117 (2013), arXiv:1205.0585 [hep-lat].
- [59] W. Detmold and K. Orginos, *Phys. Rev.* **D87**, 114512 (2013), arXiv:1207.1452 [hep-lat].
- [60] J. Günther, B. C. Toth, and L. Varnhorst, *Phys. Rev.* **D87**, 094513 (2013), arXiv:1301.4895 [hep-lat].
- [61] H. Nemura, *Comput. Phys. Commun.* **207**, 91 (2016), arXiv:1510.00903 [hep-lat].
- [62] C. Morningstar, J. Bulava, J. Foley, K. J. Juge, D. Lenkner, M. Peardon, and C. H. Wong, *Phys. Rev.* **D83**, 114505 (2011), arXiv:1104.3870 [hep-lat].
- [63] M. Peardon, J. Bulava, J. Foley, C. Morningstar, J. Dudek, R. G. Edwards, B. Joo, H.-W. Lin, D. G. Richards, and K. J. Juge (Hadron Spectrum), *Phys. Rev.* **D80**, 054506 (2009), arXiv:0905.2160 [hep-lat].
- [64] A. Hartono, A. Sibiryakov, M. Nooijen, G. Baumgartner, D. Bernholdt, S. Hirata, C. Lam, R. Pitzer, J. Ramanujam, and P. Sadayappan, *Automated Operation Minimization of Tensor Contraction Expressions in Electronic Structure Calculations*, Tech. Rep. OSU-CISRC-2/05-TR10 (Dept. of Computer Science and Engineering, The Ohio State University, 2005).
- [65] A. Hartono, Q. Lu, X. Gao, S. Krishnamoorthy, M. Nooijen, G. Baumgartner, D. E. Bernholdt, V. Choppella, R. M. Pitzer, J. Ramanujam, A. Rountev, and P. Sadayappan, in *Computational Science – ICCS 2006*, edited by V. N. Alexandrov, G. D. van Albada, P. M. A. Sloot, and J. Dongarra (Springer Berlin Heidelberg, Berlin, Heidelberg, 2006) pp. 267–275.
- [66] A. Hartono, Q. Lu, T. Henretty, S. Krishnamoorthy, H. Zhang, G. Baumgartner, D. E. Bernholdt, M. Nooijen, R. Pitzer, J. Ramanujam, and P. Sadayappan, *The Journal of Physical Chemistry A* **113**, 12715 (2009), pMID: 19888780, <https://doi.org/10.1021/jp9051215>.
- [67] R. N. C. Pfeifer, J. Haegeman, and F. Verstraete, *Phys. Rev. E* **90**, 033315 (2014).
- [68] https://github.com/laphnn/contraction_optimizer.
- [69] C. Morningstar, J. Bulava, B. Fahy, J. Foley, Y. Jhang, *et al.*, *Phys. Rev.* **D88**, 014511 (2013), arXiv:1303.6816 [hep-lat].
- [70] W. Wilcox, in *Numerical challenges in lattice quantum chromodynamics. Proceedings, Joint Interdisciplinary Workshop, Wuppertal, Germany, August 22-24, 1999* (1999) pp. 127–141, arXiv:hep-lat/9911013 [hep-lat].
- [71] J. Foley, K. Jimmy Juge, A. O’Cais, M. Peardon, S. M. Ryan, and J.-I. Skullerud, *Comput. Phys. Commun.* **172**, 145 (2005), arXiv:hep-lat/0505023 [hep-lat].
- [72] C. Morningstar and M. J. Peardon, *Phys. Rev.* **D69**, 054501 (2004), arXiv:hep-lat/0311018 [hep-lat].
- [73] M. Bruno *et al.*, *JHEP* **02**, 043 (2015), arXiv:1411.3982 [hep-lat].
- [74] M. Bruno, T. Korzec, and S. Schaefer, *Phys. Rev.* **D95**, 074504 (2017), arXiv:1608.08900 [hep-lat].
- [75] M. Lüscher and S. Schaefer, *JHEP* **07**, 036 (2011), arXiv:1105.4749 [hep-lat].
- [76] A. Gérardin, M. Cè, G. von Hippel, B. Hörz, H. B. Meyer, D. Mohler, K. Ottnad, J. Wilhelm, and H. Wittig, (2019), arXiv:1904.03120 [hep-lat].
- [77] <https://github.com/ebatz/jupan>.
- [78] C. Michael and I. Teasdale, *Nucl. Phys.* **B215**, 433 (1983).
- [79] B. Blossier, M. Della Morte, G. von Hippel, T. Mendes, and R. Sommer, *JHEP* **04**, 094 (2009), arXiv:0902.1265 [hep-lat].
- [80] C. Morningstar, J. Bulava, B. Singha, R. Brett, J. Fallica, A. Hanlon, and B. Hörz, *Nucl. Phys.* **B924**, 477 (2017), arXiv:1707.05817 [hep-lat].

- [81] B. Ananthanarayan, G. Colangelo, J. Gasser, and H. Leutwyler, Phys. Rept. **353**, 207 (2001), arXiv:hep-ph/0005297 [hep-ph].
- [82] S. R. Beane, W. Detmold, and M. J. Savage, Phys. Rev. **D76**, 074507 (2007), arXiv:0707.1670 [hep-lat].
- [83] W. Detmold and M. J. Savage, Phys. Rev. **D77**, 057502 (2008), arXiv:0801.0763 [hep-lat].
- [84] M. T. Hansen and S. R. Sharpe, Phys. Rev. **D93**, 096006 (2016), arXiv:1602.00324 [hep-lat].
- [85] S. R. Sharpe, Phys. Rev. **D96**, 054515 (2017), [Erratum: Phys. Rev. D98, no. 9, 099901 (2018)], arXiv:1707.04279 [hep-lat].
- [86] J.-Y. Pang, J.-J. Wu, H. W. Hammer, U.-G. Meißner, and A. Rusetsky, Phys. Rev. **D99**, 074513 (2019), arXiv:1902.01111 [hep-lat].
- [87] The numerical constants appearing in this expression are evaluated in appendices A and C of [84].
- [88] M. Mai, private communication.
- [89] R. G. Edwards and B. Joo (SciDAC), Nucl. Phys. Proc. Suppl. **140**, 832 (2005).
- [90] S. Hashimoto, PTEP **2017**, 053B03 (2017), arXiv:1703.01881 [hep-lat].
- [91] M. T. Hansen, H. B. Meyer, and D. Robaina, Phys. Rev. **D96**, 094513 (2017), arXiv:1704.08993 [hep-lat].
- [92] J. Bulava and M. T. Hansen, (2019), arXiv:1903.11735 [hep-lat].

Three-pion interpolating operators

The interpolators used in this work are given in Tables II to V for zero and nonzero total momenta. In practice, the normalization of an interpolator along each row of the tables is arbitrary. Correlation functions for equivalent total momenta are averaged, and the corresponding interpolators can be obtained using the reference rotations given in Ref. [69] of the main text.

TABLE II. Interpolating operators in the form of Eq. (3) with total momentum $\mathbf{d} = [000]$ transforming according to row μ of irrep Λ . Each row corresponds to one interpolator in terms of the elementals in the column heading with coefficient given in the table. Empty entries indicate a vanishing coefficient.

Λ	μ	$[000] [-00] [++0]$	$[000] [0-0] [0+0]$	$[000] [00-] [00+]$	$[000] [000] [000]$	$[000] [00+] [00-]$	$[000] [0+0] [0-0]$	$[000] [+00] [-00]$
A_{1u}^-	1	1	1	1		1	1	1
E_u^-	1	$-\sqrt{3}$	$\sqrt{3}$		1		$\sqrt{3}$	$-\sqrt{3}$
	2	1	1	-2		-2	1	1

Algorithm for operation-count minimization

The relevant correlation functions are evaluated through tensor contractions of the rank-2 meson functions defined in Eq. (5) as shown in Eq. (6) of the

TABLE III. Same as Table II but for $\mathbf{d} = [001]$.

Λ	μ	$[000] [+0+] [000]$	$[0-0] [0++] [000]$	$[000] [00+] [00+]$	$[0+0] [0-+] [000]$	$[+00] [-0+] [000]$
A_2^-	1			1		
B_2^-	1	1	1		1	1
			-1		-1	1

TABLE IV. Same as Table II but for $\mathbf{d} = [011]$.

Λ	μ	$[000] [-00] [+++]$	$[000] [000] [0++]$	$[000] [00+] [0+0]$	$[000] [0+0] [00+]$	$[000] [+00] [-++]$
A_2^-	1	1		1	1	1
B_2^-	1	1	1			-1

TABLE V. Same as Table II but for $\mathbf{d} = [111]$.

Λ	μ	$[000] [000] [+++]$	$[000] [0+0] [+0+]$	$[000] [0++] [+00]$	$[000] [+0+] [0+0]$	$[000] [+00] [00+]$	$[000] [00+] [0+0]$	$[000] [0+0] [00+]$	$[000] [00+] [0+0]$	$[000] [0+0] [00+]$
A_2^-	1					1	1	1	1	1
		1				1	1	1	1	1
E^-	1		1	1	-2					
	2	$\sqrt{3}$	$-\sqrt{3}$							

main text for the single-pion correlation function. For multi-pion correlation functions, linear combinations of products of these meson functions with various momenta, but the same total momentum, are required to compute correlation functions in a definite irrep according to the Clebsch-Gordan coefficients discussed in the main text. In the following we refer to an expression in terms of tensor contractions for a given pair of source and sink times, and each meson function with a single noise combination and momentum, as a diagram.

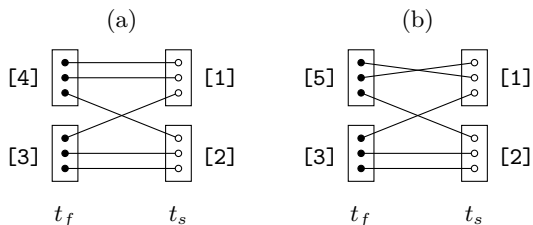
The method we use to reduce the operation count required for the evaluation of tensor contractions was proposed in the context of quantum chemistry (Refs. [64–66] in the main text) and consists of two parts.

In the first part, for a given diagram, using pairwise contraction of two tensors over all joint indices as the elemental computational kernel, the list of possible locally optimal next computational steps is determined by requiring that the proposed step remove as many contractions as possible at the lowest cost. This step is irrelevant for multi-meson correlation functions as all contractions have complexity of either N_{dii}^2 if both in-

dices are contracted over or N_{dil}^3 if only one index is contracted with two spectator indices; this step is however useful in meson-baryon and baryon-baryon correlation function construction where the arithmetic operation count is reduced by powers of N_{dil} through judicious choice of the order of elemental contractions. This in-diagram optimization is for instance implemented in the `einsum` function which ships with `numpy` (https://github.com/dgasmith/opt_einsum).

In the second part, each of the locally optimal proposed steps is ranked against all diagrams to identify the step which appears most frequently as a subexpression globally. The best-ranking contraction is performed and the resulting intermediary object substituted in all relevant diagrams, thereby reducing the number of contractions required to compute the whole set of correlation functions compared to computing diagrams individually. This procedure is referred to as common subexpression elimination (CSE) for instance in compiler design.

As a simple example, consider the list of two diagrams to compute shown below.



They involve five baryon functions, i.e. rank-3 tensors, each with a definite momentum, irrep and noise combination labeled one to five. The most straightforward way to evaluate those two diagrams is to combine tensors on the source and sink times into outer products and perform the resulting contractions in both diagrams at a cost of $2N_{\text{dil}}^6$.

According to the first step of the algorithm discussed above, a better way to evaluate the single diagram (a) proceeds as follows. Viewing pairwise contraction of two tensors over all common indices as the computational kernel, there are four possible steps:

contraction step	removed indices	step complexity
[2] – [3]	2	N_{dil}^4
[1] – [4]	2	N_{dil}^4
[1] – [3]	1	N_{dil}^5
[2] – [4]	1	N_{dil}^5

The step complexity is given by the number of summed indices plus the number of spectator indices. The first and second line are the locally good choices in this greedy algorithm, as they reduce the number of remaining contractions the most and at the smallest cost. Labeling the resulting rank-2 tensor from either of those as a new intermediary [6] transforms diagram (a) into a diagram with

TABLE VI. Number of elemental contractions with given complexity in N_{dil} required to compute all correlation functions used in this work for a fixed time separation on a single gauge configuration with and without common subexpression elimination (CSE) and diagram consolidation (DC). Diagram consolidation does not reduce the number of required contractions when CSE is used, but speeds up the optimization process.

	N_{dil}^2	N_{dil}^3
w/o CSE, w/o DC	36,860,400	44,042,400
w/o CSE, w/ DC	10,035,600	11,810,400
w/ CSE	2,789,370	761,093

contractions between two rank-3 tensors and one rank-2 tensor remaining. Iterating this process shows that each of the two diagrams can be evaluated with complexity $2N_{\text{dil}}^4 + N_{\text{dil}}^2$.

The second step of the algorithm exploits the freedom to choose between the two locally good steps in order to reduce the global operation count. In this example, the contraction [2] – [3] can be re-used in diagram (b), whereas [1] – [4] cannot. Therefore the first step is more beneficial, and the corresponding subexpression, which only has to be computed once, is replaced with the intermediary [6] in both diagrams.

The two diagrams can thus be computed with complexity $3N_{\text{dil}}^4 + 2N_{\text{dil}}^2$, saving one of the computationally dominant contractions.

In order to speed up this optimization process for the large number of diagrams required in this work, duplicate diagrams are eliminated in a preprocessing step, which we refer to as diagram consolidation (DC). Duplicate diagrams are produced when a given momentum combination appears in the Clebsch-Gordan coefficients for more than one irrep (e.g. for the $\pi(0)\pi(1)\pi(1)$ operators in the irreps A_{1u}^- and E_u^- with zero total momentum), or in the course of noise averaging (e.g. for the ground-state interpolator in A_{1u}^-).

The number of elemental contractions required to compute all the correlation functions used in this work are given in Table VI. In total, 20,679,840 diagrams had to be evaluated, of which 15,013,440 were consolidated before optimizing the computation of the remaining diagrams. After consolidation of diagrams, employing CSE reduces the operation count by roughly a factor of 15 for the computationally dominant contractions which scale like N_{dil}^3 .

Summary of $I = 2$ $\pi\pi$ scattering results from lattice QCD

A comparison of the scattering length a_0 and effective range r_0 obtained in this work to previous determinations

TABLE VII. Comparison of the effective range obtained in this work to other lattice calculations. For convenience, the scattering length is shown as well. References are given in the main text.

m_π [MeV]	$m_\pi a_0$	$m_\pi r_0$	Ref.	Notes
200	0.1019(88)	9.0(2.4)	this work	
396	0.230(19)	12.9(3.3)	[11]	Fit A
396	0.226(19)	18.1(5.3)	[11]	Fit B
396	0.307(13)	-0.26(13)	[15]	
282	0.149(10)	21(6)	[20]	$L/a = 32, 24, 20$
282	0.154(15)	8(15)	[20]	$L/a = 32, 24$
233	0.064(12)	18.1(8.4)	[22]	

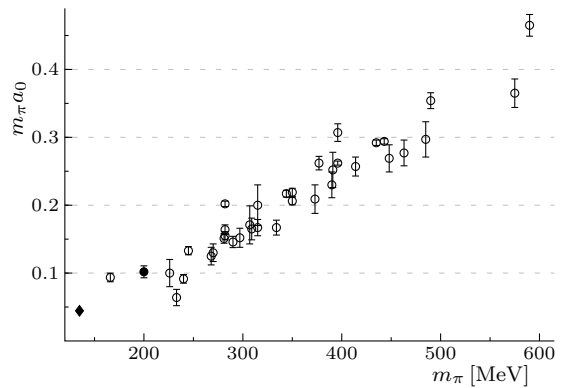


FIG. 5. Comparison of the scattering lengths extracted here (filled circle) with various lattice calculations. The filled diamond corresponds to the experimental value determined via Roy equations. The references are given in the main text.

from lattice QCD is shown in Figure 5 and Table VII, respectively. These results do not account for the discretization effects inherent to the different actions used by the various groups. The references are given in the main text.

Covariance matrix

All energies and their uncertainties, as well as their normalized covariances, for the single-pion mass, the $I = 2$ two-pion spectrum and the $I = 3$ three-pion spectrum are given in Table VIII. The single-pion mass in the first row is given in lattice units. The scale setting for the D200 ensemble employed here is discussed in Ref. [74] of the main text. All other energies are quoted in units of the single-pion mass.

TABLE VIII. Complete spectrum and normalized covariances. Different isospin sectors are separated by large row spacing into $I = 1$ (a single pion at rest), $I = 2$ and $I = 3$. The central values and uncertainties of center-of-mass energies E_{cm}/m_π in the second column are measured in units of the pion mass except for the single-pion energy in the first row, which is given in lattice units. The irrep labels are formatted as in Fig. 4.

$A_{1u}^-(0)$.06504(33)	1																																		
$A_{1g}^+(0)$	2.0172(17)	- .156	1																																	
	3.715(14)	- .944	.146	1																																
	4.897(23)	- .920	.179	.873	1																															
$E_g^+(0)$	3.624(13)	- .974	.194	.922	.902	1																														
	4.720(21)	- .992	.147	.935	.915	.962	1																													
$A_1^+(1)$	2.4082(41)	- .796	.398	.765	.741	.785	.784	1																												
	4.010(16)	- .969	.190	.929	.916	.947	.962	.776	1																											
	4.780(19)	- .982	.167	.923	.906	.958	.975	.777	.951	1																										
$B_1^+(1)$	3.889(15)	- .968	.181	.919	.905	.960	.959	.782	.943	.957	1																									
$A_1^+(2)$	2.6280(49)	- .837	.336	.805	.780	.831	.830	.725	.834	.833	.831	1																								
	2.9549(85)	- .952	.191	.932	.873	.934	.940	.829	.926	.928	.928	.828	1																							
	4.125(16)	- .991	.156	.940	.916	.966	.984	.791	.959	.974	.961	.829	.942	1																						
$A_1^+(2)$	4.208(16)	- .993	.164	.939	.914	.970	.986	.793	.965	.979	.967	.837	.947	.985	1																					
$B_1^+(2)$	4.091(16)	- .994	.161	.940	.919	.964	.988	.788	.963	.978	.964	.831	.945	.987	.990	1																				
$A_1^+(3)$	2.7868(80)	- .664	.276	.628	.604	.661	.657	.556	.678	.660	.652	.635	.672	.657	.671	.665	1																			
	3.344(12)	- .915	.172	.896	.857	.893	.905	.769	.910	.904	.899	.808	.913	.909	.912	.906	.664	1																		
$E^+(3)$	3.246(10)	- .971	.201	.916	.896	.953	.963	.774	.947	.956	.948	.846	.937	.965	.968	.967	.687	.902	1																	
$A_1^+(4)$	2.0133(29)	- .011	.310	.048	.059	.048	- .003	.144	.035	.036	.076	.190	.108	.027	.034	.023	.104	.085	.128	1																
	2.924(10)	- .557	.215	.546	.586	.570	.548	.471	.565	.582	.592	.524	.540	.570	.567	.566	.427	.539	.565	.240	1															
$B_1^+(4)$	3.674(15)	- .898	.164	.878	.849	.887	.879	.722	.890	.883	.886	.796	.876	.896	.895	.890	.605	.859	.889	.105	.547	1														
$A_1^+(4)$	3.628(13)	- .986	.143	.932	.914	.955	.988	.768	.956	.972	.957	.831	.933	.982	.985	.985	.649	.899	.961	.020	.564	.883	1													
	3.0478(60)	- .164	.813	.164	.164	.182	.159	.462	.180	.155	.158	.268	.197	.160	.162	.168	.184	.172	.153	.102	.083	.149	.142	1												
	4.780(17)	- .841	.130	.901	.772	.829	.828	.749	.831	.817	.832	.717	.877	.839	.843	.836	.561	.818	.815	.114	.516	.786	.826	.157	1											
$E^-(0)$	4.691(15)	- .926	.305	.887	.854	.947	.915	.877	.898	.908	.911	.822	.930	.918	.921	.917	.640	.873	.909	.111	.540	.848	.905	.317	.846	1										
$A_2^-(1)$	3.5838(85)	- .606	.525	.591	.571	.603	.596	.907	.602	.592	.602	.587	.638	.600	.609	.600	.385	.595	.571	.135	.365	.542	.576	.653	.578	.717	1									
	5.131(18)	- .916	.258	.900	.853	.906	.904	.825	.929	.900	.902	.858	.921	.903	.911	.910	.677	.885	.894	.111	.553	.859	.897	.268	.848	.911	.662	1								
$B_2^-(1)$	5.008(17)	- .901	.271	.860	.831	.900	.888	.834	.877	.888	.929	.849	.905	.890	.897	.894	.631	.857	.883	.098	.548	.819	.885	.285	.820	.922	.691	.895	1							
$A_2^-(2)$	3.8840(96)	- .661	.475	.654	.590	.672	.647	.684	.666	.649	.658	.871	.702	.650	.658	.656	.592	.661	.678	.229	.406	.620	.645	.443	.602	.721	.610	.751	.771	1						
	4.206(11)	- .874	.298	.861	.807	.867	.860	.910	.856	.849	.852	.794	.937	.869	.872	.868	.611	.852	.861	.159	.507	.817	.850	.332	.852	.923	.764	.899	.878	.721	1					
$B_2^-(2)$	5.313(19)	- .886	.233	.863	.814	.887	.872	.741	.878	.875	.872	.812	.892	.885	.886	.880	.815	.883	.899	.157	.530	.836	.866	.174	.799	.866	.540	.874	.832	.694	.827	1				
$A_2^-(3)$	5.258(19)	- .895	.233	.844	.820	.887	.886	.759	.888	.887	.888	.810	.892	.885	.894	.899	.817	.874	.900	.128	.549	.823	.879	.191	.786	.876	.562	.874	.865	.703	.841	.915	1			
$A_2^-(3)$	4.088(18)	- .416	.348	.376	.365	.420	.406	.445	.445	.415	.415	.427	.430	.413	.398	.421	.417	.624	.399	.413	.121	.252	.356	.393	.351	.369	.453	.398	.475	.476	.457	.389	.492	.518	1	
	4.608(14)	- .840	.253	.827	.769	.830	.826	.775	.818	.829	.831	.822	.881	.833	.837	.833	.830	.646	.904	.834	.139	.519	.796	.819	.262	.790	.861	.628	.877	.870	.766	.845	.840	.834	.475	1
	4.850(17)	- .914	.176	.905	.840	.898	.903	.817	.893	.892	.810	.967	.906	.913	.908	.639	.902	.900	.144	.533	.843	.895	.181	.867	.903	.626	.903	.879	.693	.927	.866	.862	.396	.870	1	
$E^-(3)$	4.528(14)	- .826	.281	.794	.742	.814	.807	.817	.798	.805	.809	.797	.841	.814	.817	.824	.631	.792	.836	.125	.455	.760	.800	.330	.750	.853	.686	.832	.777	.835	.788	.806	.481	.844	.825	1